DORNBERGER-SCHIFF, K. & GRELL, H. (1982). *Acta Cryst.* A**38**, 491–498.
DORNBERGER-SCHIFF, K. & GRELL-NIEMANN, H. (1961). *Acta Cryst.* **14**, 167–177.
DRITS, V. A. & KARAVAN, YU. V. (1969). *Acta Cryst.* B**25**, 632–639.
ĎUROVIČ, S. (1974). *Acta Cryst.* B**30**, 76–78.
ĎUROVIČ, S. & DORNBERGER-SCHIFF, K. (1976). 7th Conference on Clay Mineralogy and Petrology, Karlovy Vary, pp. 25–34.
ĎUROVIČ, S. & DORNBERGER-SCHIFF, K. (1978). *Acta Cryst.* A**34**, S8.
ĎUROVIČ, S. & DORNBERGER-SCHIFF, K. (1979). 8th Conference on Clay Mineralogy and Petrology, Teplice, pp. 19–25.
GRELL, H. & DORNBERGER-SCHIFF, K. (1982). *Acta Cryst.* A**38**, 49–54.
LISTER, J. S. & BAILEY, S. W. (1967). *Am. Mineral.* **52**, 1614–1631.
MIKLOŠ, D. (1975). *Symmetry and Polytypism of Trioctahedral Kaolin-Type Minerals* (in Slovak). CSc. Thesis, Institute of Inorganic Chemistry, Slovak Academy of Sciences, Bratislava.
WEISS, Z. & ĎUROVIČ, S. (1980). *Acta Cryst.* A**36**, 633–640.
WEISS, Z. & MIKLOŠ, D. (1979). 8th Conference on Clay Mineralogy and Petrology, Teplice, pp. 105–110.
ZVYAGIN, B. B. (1967). *Electron Diffraction Analysis of Clay Minerals*. New York: Plenum.
ZVYAGIN, B. B. (1974). Collect. Abstr. 2nd ECM, Keszthely, Hungary, pp. 162–164.
ZVYAGIN, B. B., VRUBLEVSKAYA, Z. V., ZHOUKHLISTOV, A. P., SIDORENKO, O. V., SOBOLEVA, S. V. & FEDOTOV, A. V. (1979). *Vysokovol'tnaya Elektronografiya v Issledovanii Sloistykh Mineralov*. Moscow: Nauka.

Acta Cryst. (1983). B**39**, 552–557

Chlorite Polytypism. II. Classification and X-ray Identification of Trioctahedral Polytypes

BY Z. WEISS

Coal Research Institute, 716 07 *Ostrava-Radvanice, Czechoslovakia*

AND S. ĎUROVIČ

Institute of Inorganic Chemistry, Slovak Academy of Sciences, 842 36 *Bratislava, Czechoslovakia*

(*Received* 1 *October* 1981; *accepted* 20 *April* 1983)

Abstract

Classification and identification criteria are presented for tri-trioctahedral chlorite polytypes. According to the diffractions hkl ($k = 3n$) and $0kl$ ($k \neq 3n$) they can be categorized into four subfamilies and eight MDO (maximum degree of order) groups, respectively. Each subfamily has its characteristic superposition structure, each MDO group its characteristic ***YZ*** projection – geometrical properties of these can be derived from the fully descriptive polytype symbols. Identification diagrams for single-crystal specimens (taking into account also the variability in the chemical composition) are given for one- and two-layer polytypes. Characteristic properties of powder diffraction patterns useful for identification purposes are also given.

1. Introduction

Identification of chlorite polytypes is complicated by the variability in their chemical composition, which has to be taken into consideration, in contrast to vermiculites (Weiss & Ďurovič, 1980) whose composition lies within narrow limits. Accordingly, the aim of this paper is to respect this fact when working out identification criteria for chlorite polytypes. The basis for this task are lists of MDO polytypes derived in part I (Ďurovič, Dornberger-Schiff & Weiss, 1983). Since the majority of natural chlorite specimens identified so far are trioctahedral, only these will be considered in the following.

2. Geometrical background for classification of chlorite polytypes

It is commonly known that diffraction patterns of chlorites consist of two sets of diffractions. Those with $k = 3n$ (orthogonal indexing) are always sharp, whereas those with $k \neq 3n$ are sharp only for periodic polytypes. According to Brown & Bailey (1962) the diffractions with $k = 3n$ and $h \neq 3n$ are characteristic for each of their four assemblages I*a*, I*b*, II*a*, II*b*, while the diffractions with $k \neq 3n$ are characteristic for individual polytypes.

Systematic calculations of diffraction patterns for maximum degree of order (MDO) polytypes of Mg-vermiculite (Weiss & Ďurovič, 1980) revealed that according to the diffractions with $k = 3n$, in particular

0108-7681/83/050552-06$01.50

$\pm 20l$, $\pm 13l$, the vermiculite family splits into four groups, *A*, *B*, *C*, *D*, which are analogous to Brown & Bailey's assemblages II*a*, I*a*, II*b*, I*b*, respectively. The diffractions with $k \neq 3n$, in particular $02l$, lead to classification of two-layer MDO polytypes into five MDO groups (I to V), so that, for example, the diffractions $\pm 20l$ and $02l$ suffice for their unambiguous identification. It was stated that these facts are due to a very simple geometrical background which can be explained as follows.

A Fourier series calculated with coefficents $F(hkl)$ for $k = 3n$ only corresponds to a fictitious structure whose electron density distribution $\hat{\rho}(xyz)$ is defined as

$$\hat{\rho}(xyz) = \tfrac{1}{3}[\rho(xyz) + \rho(x,y+\tfrac{1}{3},z) + \rho(x,y+\tfrac{2}{3},z)].$$

This structure has been called *superposition structure* (Dornberger-Schiff, 1964) and since the corresponding diffractions are always sharp and common to all polytypes within any of the groups *A*, *B*, *C*, *D*, the structure is triperiodic and typical for any of these groups. For obvious reasons we shall call the groups *A*, *B*, *C*, *D* *subfamilies*. Each subfamily has thus its characteristic superposition structure and, as a logical consequence, also a characteristic ***XZ*** projection.

Among the diffractions with $k \neq 3n$, characteristic for individual periodic polytypes, there are also $0kl$ and these correspond obviously to the respective ***YZ*** *projections* – all polytypes belonging to the same *MDO group* have the same ***YZ*** projection and thus also the same intensities of diffractions $02l$, $04l$ *etc.* It follows that any periodic polytype is unambiguously determined by its superposition structure and by its ***YZ*** projection and these two fundamental geometrical characteristics can be recognized by inspecting the corresponding diffractions.

Fully descriptive polytype symbols characterize the stacking mode in any polytype and thus the relevant geometrical features including its superposition structure and its ***YZ*** projection can be deduced from them. It is only necessary to find the superposition structure and ***YZ*** projection of individual kinds of building layers (BL's) in their possible orientations and set the rules for transforming displacement characters (Ďurovič, 1981).

These considerations can be applied to chlorites as follows: the superposition structure of any kind of BL has an *H* mesh (the mesh is *H*-centred, *i.e.* $x,y + [0,0; 0,\frac{1}{3}; 0,\frac{2}{3}]$); any B_{3n} as well as any pair (B_{3n+1}, B_{3n+2}) contains in it one octahedron with averaged occupation in the same orientation as in the original polytype. These BL's retain their trigonal symmetry: $H(3)1m$ for $B_{3n\pm1}$, $H(\bar{3})12/m$ for B_{3n} and they can occur in only two orientations, labelled, for example, ***E*** and ***U***, in accordance with the original orientational characters ***e*** and ***u***, respectively. With respect to the *H* mesh the three displacement vectors with even (uneven) characters will fuse into one vector denoted $\langle \boldsymbol{E} \rangle$ ($\langle \boldsymbol{U} \rangle$), the vectors $\langle + \rangle$, $\langle - \rangle$, $\langle * \rangle$ fuse into a zero vector $\langle * \rangle$. The superposition structure of any subfamily is therefore trigonal with an *H* cell.

As far as the ***YZ*** projection is concerned, its period in the ***Y*** direction is $b/2$, and any B_{3n} yields an image – labelled ***M*** – with symmetry $p2m(m)$. No matter whether its orientation was ***e*** or ***u***, any $B_{3n\pm1}$ yields an image – labelled ***V*** – with symmetry $[.m(.)]$. With respect to the halved period in the ***Y*** direction, the three displacement vectors $\langle \boldsymbol{1} \rangle$, $\langle \boldsymbol{2} \rangle$, $\langle - \rangle$ fuse into a vector denoted $\langle \boldsymbol{A} \rangle$ with *y* component $+b/6$; $\langle \boldsymbol{4} \rangle$, $\langle \boldsymbol{5} \rangle$, $\langle + \rangle$ fuse into vector $\langle \bar{\boldsymbol{A}} \rangle$ with *y* component $-b/6$ and $\langle \boldsymbol{0} \rangle$, $\langle \bar{\boldsymbol{3}} \rangle$, $\langle * \rangle$ into $\langle * \rangle$, that is zero vector. Keeping these relations in mind, we can take the symbols of all the MDO polytypes of one family one by one, carry out the corresponding transformations of characters, determine new identity periods of resulting structures and categorize them accordingly. As a result, for trioctahedral MDO polytypes, the classification as given in Table 1 has been obtained. It is easy to see that, for example, all MDO polytypes of the subfamily *A* have the same one-layer, rhombohedral superposition structure with symbol:

$$\left|\begin{matrix} E & U\,.\,U \\ * & E \quad * \end{matrix}\right|,$$

and all MDO polytypes of the MDO group IV have the same two-layer ***YZ*** projection:

$$\left|\begin{matrix} M & V\,.\,V & M & V\,.\,V \\ X & \bar{A} \quad X & X & A \quad X \\ * & & * & \end{matrix}\right|,$$

where the triplet of vectors $\langle * \rangle$, $\langle \bar{\boldsymbol{A}} \rangle$, $\langle \boldsymbol{A} \rangle$ is denoted ***X***. The recognition of the above facts simplifies greatly the computational work for obtaining individual identification diagrams.

3. X-ray identification of one- and two-layer trioctahedral polytypes

For calculation of diffraction patterns for the individual MDO polytypes, the same method was used as for Mg-vermiculite (Weiss & Ďurovič, 1980). Since these patterns are influenced by the chemical composition (Fe:Mg ratio), two chlorite representatives have been chosen:

Mg-chlorite, close to clinochlore:

$$(Mg_{4.6}Al_{1.4})(Si_{2.6}Al_{1.4})O_{10}(OH)_8;$$

Fe-chlorite, close to chamosite:

$$(Mg_{0.92}Fe_{3.68}Al_{1.4})(Si_{2.6}Al_{1.4})O_{10}(OH)_8.$$

Identical occupancy of octahedral sites within the 2:1 layers and within the interlayer hydroxide sheets was assumed. Lattice parameters were estimated according to Bailey (1972) in accordance with the chemical

Table 1. *Classification of MDO polytypes of trioctahedral chlorites*

MDO group \ Subfamily	*A*	*B*	*C*	*D*
I	e u.u x 2 x +	u u.u x 2 x +	u e.e e 1 e 5	—
II	e u.u x 0 x *	u u.u x 0 x *	u e.e e 3 e 3	u u.u e 0 e 3
III	—	—	—	u u.u e 2 e 1
IV	u e.e u e.e x 5 x x 1 x * *	e e.e e e. e x 5 x x 1 x * *	e u.u e u.u u 2 u u 4 u 0 0	u u.u u u.u e 4 e e 2 e 3 3
V	u e.e u e.e x 3 x x 3 x + −	e e.e e e.e x 3 x x 3 x + −	e u.u e u.u u 0 u u 0 u 2 4	u u.u u u.u e 0 e e 0 e 1 5
VI	u e.e u e.e u e.e x 3 x x 5 x x 1 x * * *	e e.e e e.e e e.e x 3 x x 5 x x 1 x * * *	—	—
VII	—	—	u e.e u e.e u e.e e 3 e e 5 e e 1 e 5 3 1	—
VIII	—	—	—	e e.e e e.e e e.e u 3 u u 5 u u 1 u 2 4 0

composition, taking into account also the lattice geometry of the polytype.

The one-layer and two-layer polytypes have been studied most often. Therefore, only these will be dealt with in the following. The indexing of their diffraction patterns refers to their actual unit cells, defined for individual polytypes by one of the choices given in Table 2. The analysis of the results thus obtained confirmed those discussed in the previous section: the subdivision into four subfamilies according to the diffractions $\pm 20l$ or $\pm 13l$. From the geometrical properties of superposition structures it follows that this classification also includes other, non-MDO periodic as well as disordered polytypes assuming no intermixing of packet types in them. The diffractions $\pm 20l$ and $\pm 13l$ are relatively strong and the distribution of their intensities for any of the subfamilies *A*, *B*, *C*, *D* is so characteristic that each subfamily can be determined simply by a comparison of observed intensities with calculated values. In Fig. 1 visual representations of $|F|^2$ for diffractions $\pm 20l$ are given for subfamilies *A*, *B*, *C*, *D* for an Mg-chlorite. Visual representations for Fe-chlorite are given in the deposited material.* It is immediately apparent that the respective distributions

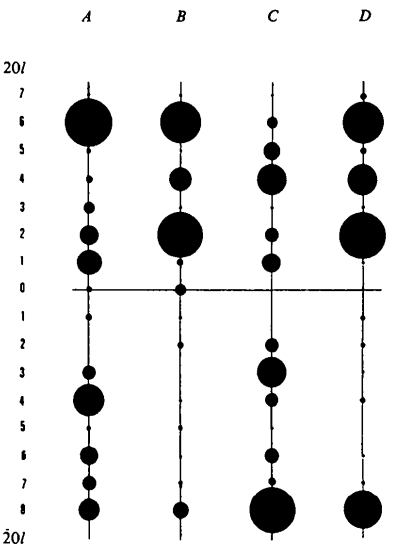

Fig. 1. Visual representation of calculated $|F|^2$ values (the strongest $|F|^2$ value of each subfamily is drawn as the biggest circle) for characteristic diffractions $\pm 20l$ of MDO polytypes of Mg-chlorite and their classification into the subfamilies *A*, *B*, *C* and *D*. The indexing refers to actual one-layer unit cells.

of intensities are influenced by subfamily much more than by chemical composition. The distinguishing between polytypes of the subfamily *B* and those of the subfamily *D* is greatly simplified by their lattice geometries (see Table 2). Thus, the indexing refers to

* The complete manuscript has been deposited with the British Library Lending Division as Supplementary Publication No. SUP 38517 (26 pp.). Copies may be obtained through The Executive Secretary, International Union of Crystallography, 5 Abbey Square, Chester CH1 2HU, England.

Table 2. *Lattice parameters of the polytypes used for calculation of diffraction patterns*

Lattice geometry			Mg-chlorite $a = 5{\cdot}323$ Å $b = 9{\cdot}220$ Å			Fe-chlorite $a = 5{\cdot}383$ Å $b = 9{\cdot}323$ Å		
			c (Å)	α (°)	β (°)	c (Å)	α (°)	β (°)
(*a*)	Polytypes of the subfamilies *A*, *B*, *C*	1-layer	14·255	90	97·15	14·258	90	97·23
		2-layer	28·510	90	97·15	28·516	90	97·23
(*b*)	Polytypes of the subfamily *D* (without *D*/III)	1-layer	14·144	90	90	14·144	90	90
		2-layer	28·288	90	90	28·288	90	90
(*c*)	Polytype *D*/III	1-layer	14·474	102·26	90	14·481	102·39	90

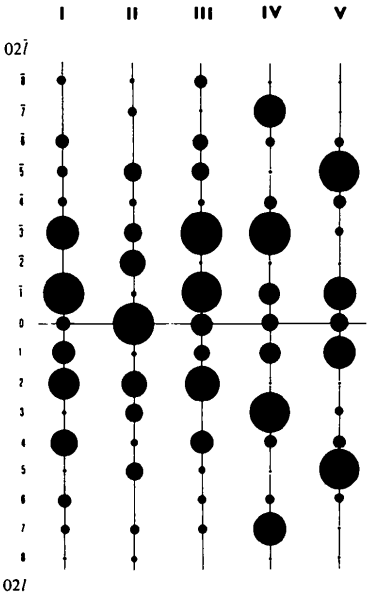

Fig. 2. Visual representation of calculated $|F|^2$ values (the strongest $|F|^2$ value of each group is drawn as the biggest circle) for characteristic diffractions 02*l* in one- and two-layer MDO polytypes of chlorite and their classification into the MDO groups I to V.

different unit cells. From Friedel's law and from the trigonal symmetry of any superposition structure it follows that the $|F(\pm 13l)|^2$ values are closely related to those of $|F(\pm 20l)|^2$ so that $|F(\pm 13l)|^2$ values can be deduced from the $|F(\pm 20l)|^2$ values shown in Fig. 1. This may also be important for the purposes of identification. The above relations are given in the deposited material.*

The variability of chemical composition of trioctahedral chlorites resulting from their isomorphism may induce changes in their X-ray diffraction patterns owing to different scattering powers of atoms. The intensities of diffractions 02*l*, 04*l*, $\pm 11l$, $\pm 15l$, $\pm 22l$, $\pm 24l$, $\pm 31l$ (for all *l*), $\pm 33l$, $\pm 13l$ (for *l* even) and $\pm 20l$, 00*l*, 06*l* (for *l* odd) are independent of the Fe:Mg ratio in octahedral positions for identical occupancy of octahedral sites within the 2:1 layers and within the interlayer hydroxide sheets. However, the intensities of diffractions $\pm 33l$, $\pm 13l$ (for *l* odd) and $\pm 20l$, 00*l*, 06*l* (for *l* even) are dependent on the Fe:Mg ratio. The changes of $|F|$ values for selected types of diffractions resulting from Fe content in the octahedral positions are quantified in the deposited material.*

According to the diffractions 02*l* and/or 04*l* which characterize the ***YZ*** projection of structure, any one- and two-layer MDO polytype can be assigned to one of the MDO groups I, II, III, IV, V, independent of its chemical composition. Fig. 2 shows calculated $|F(02l)|^2$ values for them.

These identification criteria make it possible to determine unambiguously one- and two-layer MDO polytypes if their subfamily and MDO groups are determined. We shall designate it as *A*/I, *B*/II *etc.* For determination of subfamily and MDO group, the diffractions $\pm 20l$ and/or $\pm 13l$ – using Fig. 1 – and 02*l* (Fig. 2), respectively, are best suited.

4. Powder diffraction patterns

Although the calculated diffraction patterns are based on idealized symmetry of chlorite polytypes and varied with their chemical composition, we believe that partial identification (*i.e.* determination of the subfamily) can be made from powder diffraction patterns. The identification can be based on a determinative part of the pattern, such as in Figs. 3 and 4, containing the $\pm 20l$ and $\pm 13l$ diffractions but no intensive basal peaks. It is possible to model powder patterns for any chemical composition, and use the determinative parts of such patterns for identifying the subfamily.* As far as unambiguous determination of polytype from powder diffraction patterns is concerned, we are not very optimistic, since the intensities of the most important diffractions of 02*l* (04*l*) are influenced by disorder and their intensities are relatively low.

* See deposition footnote.

* See deposition footnote.

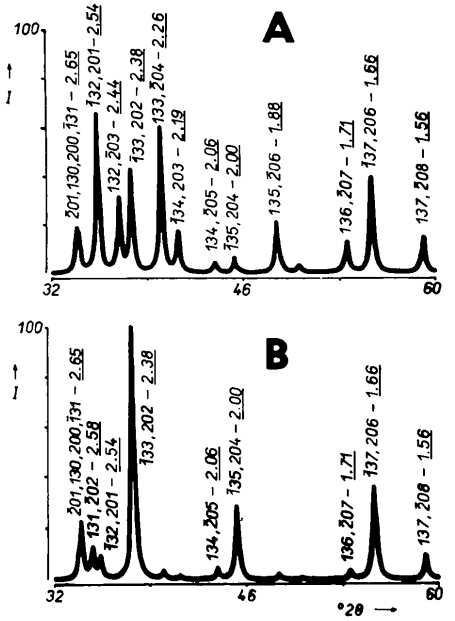

Fig. 3. Determinative part of the calculated powder diffraction patterns (experimental arrangement: diffractometer, Cu radiation, random orientation of particles in the sample) of MDO polytypes of Mg-chlorite belonging to subfamilies *A* and *B*. The indexing refers to actual one-layer cells.

5. Examples

A comparison of the characteristic $|F(\pm 20l)|^2$ and $|F(02l)|^2$ values calculated from the crystal data published by Shirozu & Bailey (1965) with the theoretical values calculated for Fe-chlorite (see Fig. 5) indicates unambiguously the MDO polytype *D*/II with the symbol

$$\left|\begin{matrix} u & u.u \\ e & 0 \quad e \end{matrix}\right|_3.$$

Similar results* have been obtained also for structural data published by Brown & Bailey (1963), Joswig, Fuess, Rothbauer, Takéuchi & Mason (1980), Steinfink (1958*a*,*b*, 1962) and Phillips, Loveless & Bailey (1980).

Brown & Bailey (1962) determined relative abundances of one-layer chlorite polytypes in 303 natural samples. Our interpretation of these results is that 290 of them can be described using derived MDO polytypes: mostly *C*/I and *C*/II (243 samples), followed by *D*/II (37 samples) and *B*/I and *B*/II (10 samples).

The authors wish to express their thanks to Drs M. Rieder and B. Čičel and to Professor K. Dornberger-Schiff for discussions and critical comments.

* See deposition footnote.

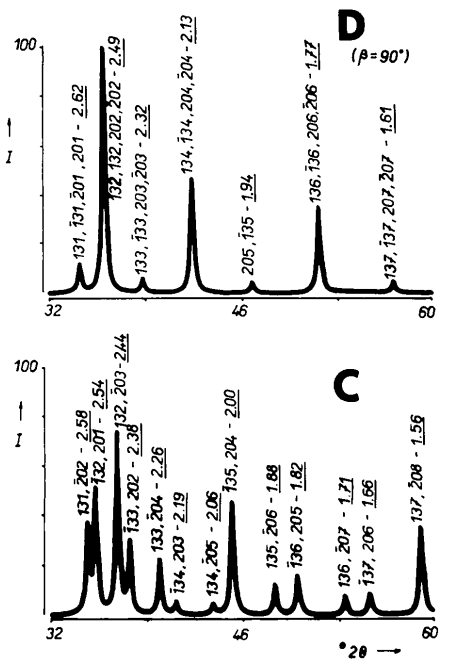

Fig. 4. Determinative part of the calculated powder diffraction patterns (experimental arrangement: diffractometer, Cu radiation, random orientation of particles in the sample) of MDO polytypes of Mg-chlorite belonging to subfamilies *C* and *D*. The indexing refers to actual one-layer cells.

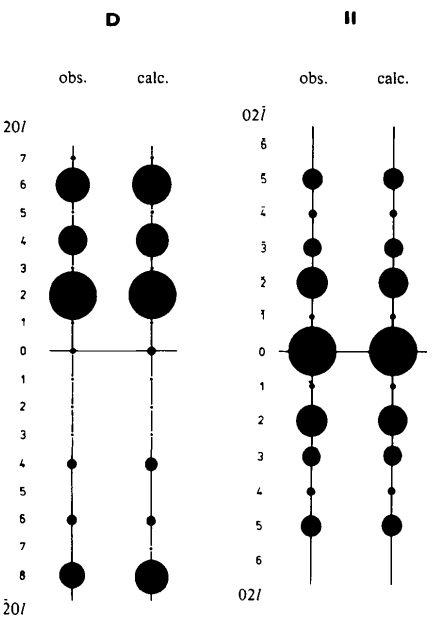

Fig. 5. Comparison of the characteristic $|F(\pm 20l)|^2$ and $|F(02l)|^2$ values calculated from the data of Shirozu & Bailey (1965) (obs.) with the theoretical values calculated for Fe-chlorite and MDO polytype *D*/II (calc.). $|F|^2$ values are normalized to the strongest diffraction.

References

BAILEY, S. W. (1972). *Clays Clay Miner.* **20**, 381–388.
BROWN, B. E. & BAILEY, S. W. (1962). *Am. Mineral.* **47**, 819–850.
BROWN, B. E. & BAILEY, S. W. (1963). *Am. Mineral.* **48**, 42–61.
DORNBERGER-SCHIFF, K. (1964). *Abh. Dtsch. Akad. Wiss. Berlin Kl. Chem. Geol. Biol.* **3**.
ĎUROVIČ, S. (1981). *Fortschr. Mineral.* **59**, 191–226.
ĎUROVIČ, S., DORNBERGER-SCHIFF, K. & WEISS, Z. (1983). *Acta Cryst.* B**39**, 547–552.
JOSWIG, W., FUESS, H., ROTHBAUER, R., TAKÉUCHI, Y. & MASON, S. A. (1980). *Am. Mineral.* **65**, 349–353.
PHILLIPS, T. L., LOVELESS, J. K. & BAILEY, S. W. (1980). *Am. Mineral.* **65**, 112–122.
SHIROZU, H. & BAILEY, S. W. (1965). *Am. Mineral.* **50**, 868–885.
STEINFINK, H. (1958*a*). *Acta Cryst.* **11**, 191–195.
STEINFINK, H. (1958*b*). *Acta Cryst.* **11**, 195–198.
STEINFINK, H. (1962). *Acta Cryst.* **15**, 1310.
WEISS, Z. & ĎUROVIČ, S. (1980). *Acta Cryst.* A**36**, 633–640.

Acta Cryst. (1983). B**39**, 557–561

Electron-Density Distributions in Crystals of $KMnF_3$ and $KNiF_3$

BY NAOTO KIJIMA, KIYOAKI TANAKA AND FUMIYUKI MARUMO

The Research Laboratory of Engineering Materials, Tokyo Institute of Technology, Nagatsuta 4259, *Midori-ku, Yokohama* 227, *Japan*

(*Received* 12 *February* 1983; *accepted* 4 *April* 1983)

Abstract

The electron density distributions in crystals in $KMnF_3$ and $KNiF_3$ were investigated on the bases of the intensity data collected by diffractometry at 293 K. The refinement with aspherical scattering factors for 3*d* orbitals revealed that the Mn^{2+} ion is in the high-spin state $(t_{2g})^3(e_g)^2$ and that the Ni^{2+} ion is in the $(t_{2g})^6(e_g)^2$ state, both to good approximations. Further population refinement showed that the Mn^{2+} ion deviates slightly from the high-spin state and that the Ni^{2+} ion is in the state $(t_{2g})^{5\cdot7}(e_g)^{2\cdot3}$. The residual density map after the population refinement suggests significant anharmonic vibrations of ions in $KMnF_3$ crystals at 293 K. The present study confirms that accurate X-ray diffraction study can detect the difference in 3*d* electron configurations. [Crystal data: $KMnF_3$: *Pm*3*m*, a = 4·1889 (7) Å, $Z = 1$, $D_x = 3{\cdot}412$ g cm^{-3}, μ(Mo $K\alpha$) = 59·35 cm^{-1}; $KNiF_3$: *Pm*3*m*, $a = 4{\cdot}0115$ (7) Å, $Z = 1$, $D_x = 3{\cdot}982$ g cm^{-3}, μ(Mo $K\alpha$) = 88·91 cm^{-1}.]

Introduction

We have performed a series of investigations on electron density distributions in crystals of KMF_3 (*M*: Mn, Fe, Co, Ni and Cu), taking the aspherical distribution of 3*d* electrons into account. In previous articles on $KCuF_3$ (Tanaka, Konishi & Marumo, 1979, 1980) and $KCoF_3$ (Kijima, Tanaka & Marumo, 1981), we have found that residual density maps change drastically according to a slight variation in the assumed configurations of *d* electrons. Distortion of electron distribution by the Jahn–Teller effect in $KCuF_3$ crystals was clearly revealed on deformation density maps. In the case of $KCoF_3$ crystals, the high-spin model deleted most of the peaks around the Co^{2+} ion on the deformation density maps, while the low-spin model gave tremendously large residual peaks. Accordingly it became evident that the spin state of the transition metals could be determined unequivocally by X-ray diffraction.

The present study was undertaken to determine the spin state of the Mn^{2+} ions in $KMnF_3$ crystals and the electron configuration of Ni^{2+} ions in $KNiF_3$ crystals by the X-ray diffraction method.

Experimental

Single crystals of $KMnF_3$ and $KNiF_3$, synthesized by the Bridgemann method and flux method respectively, were used in the present study. They were shaped into spheres by the Bond (1951) method. The lattice constants were determined from 48 2θ values for each crystal. These 2θ values were measured with a four-circle diffractometer using Mo $K\alpha_1$ radiation in the range higher than 88°, where Bragg reflexions of the Mo $K\alpha_1$ and Mo $K\alpha_2$ radiations do not interact with each other. The lattice constants are given in the *Abstract* together with other crystal data. The lattice constants are equal to those observed by Okazaki & Suemune (1961) within the experimental errors.

Intensities of reflexions in an octant of reciprocal space were collected on a Philips automated four-circle diffractometer. As to reflexions with very strong

0108-7681/83/050557-05$01.50